

Enhanced ionization in the cylindrical Hall thruster

A. Smirnov,^{a)} Y. Raitses, and N. J. Fisch

Plasma Physics Laboratory, Princeton University, P.O. Box 451, Princeton, New Jersey 08543

(Received 7 February 2003; accepted 28 April 2003)

Conventional annular Hall thrusters do not scale efficiently to low power. An alternative approach, a cylindrical Hall thruster with a cusp-type magnetic field distribution, has been investigated. A relatively large 9-cm-diam version of a cylindrical thruster, operated in 300–1000 W power range, and the 2.6 cm miniaturized cylindrical Hall thruster, operated in the power range 50–300 W, exhibited performance comparable with conventional annular Hall thrusters of the similar size. The cylindrical thrusters have unusually high propellant utilization, compared to conventional Hall thrusters. Numerical simulations, performed within the framework of a quasi-one-dimensional stationary thruster model, show that the increase in the propellant utilization does not appear to be quantitatively explained by a reduction of plasma wall losses. A more complete theoretical model, likely including kinetic effects, will be necessary to explain the observed propellant utilization effect. © 2003 American Institute of Physics. [DOI: 10.1063/1.1585114]

I. INTRODUCTION

Scaling to low-power Hall thrusters requires a discharge voltage or a discharge current to be decreased. The degree to which the first option can be accommodated is limited by the necessity to keep the exhaust ion velocity high. The second option implies that the propellant flow rate should be reduced. In order to maintain high propellant utilization efficiency at low propellant flow rates, the thruster channel must be scaled down to preserve the ionization probability. Thus, according to Ref. 1, the acceleration region length, which is mainly determined by the magnetic field distribution, must be decreased linearly together with the channel sizes, while the magnetic field must be increased inversely to the scaling factor. However, the implementation of the latter requirement is technically challenging because of magnetic saturation in the miniaturized inner parts of the magnetic core. A linear scaling down of the magnetic circuit leaves almost no room for magnetic poles or for heat shields, making difficult the achievement of the optimal magnetic fields. Nonoptimal magnetic fields result in enhanced power and ion losses, heating and erosion of the thruster parts, particularly the critical inner parts of the coaxial channel and magnetic circuit.

Currently, existing low-power Hall thruster laboratory prototypes with channel diameters 2–4 cm operate at 100–300 W power levels with efficiencies in the range of 10%–30%.^{2–4} However, further scaling of the conventional geometry Hall thruster down to subcentimeter size⁵ results in even lower efficiencies (6% at power level of about 100 W). The low efficiency might arise from a large axial electron current, enhanced either by magnetic field degradation due to excessive heating of the thruster magnets or by electron collisions with the channel walls. Thus, miniaturizing the conventional annular Hall thruster does not appear to be straightforward.

A cylindrical Hall thruster (CHT), suggested in Ref. 6, is illustrated in Fig. 1(a). The thruster consists of a boron-nitride ceramic channel, an annular anode, which serves also as a gas distributor, two electromagnetic coils, and a magnetic core. What distinguishes this thruster from conventional annular and end-Hall thrusters is the cylindrical configuration with an enhanced radial component of the cusp-type magnetic field [Fig. 1(b)]. The magnetic field lines intersect the ceramic channel walls. The electron drifts are closed, with the magnetic field lines forming equipotential surfaces, with $E = -v_e \times B$. Ion thrust is generated by the axial component of the Lorentz force, proportional to the radial magnetic field and the azimuthal electron current.

The cylindrical channel features a short annular region and a longer cylindrical region. The length of the annular region is selected to be approximately equal to an ionization mean-free path of a neutral atom. This provides high ionization of the working gas at the boundary of the annular and the cylindrical regions. In this case, most of the voltage drop occurs in the cylindrical region.

Compared to a conventional geometry (annular) Hall thruster, the CHT has lower surface-to-volume ratio and, therefore, potentially smaller wall losses in the channel. Electron losses onto the outer wall and central ceramic piece might be additionally reduced due to the magnetic mirror effect [see Fig. 1(b)]. Having potentially smaller wall losses in the channel, a CHT should suffer lower erosion and heating of the thruster parts, particularly the critical inner parts of the channel and magnetic circuit. This makes the concept of a CHT very promising for low-power applications.

A relatively large 9-cm-diam version of a cylindrical thruster exhibited performance comparable with conventional annular Hall thrusters in the subkilowatt power range.⁶ In recent work,⁷ a miniature 2.6-cm-diam CHT was studied and its performance was compared to that of the annular thruster of the same size. In the power range 50–300 W, the miniature cylindrical and annular thrusters were shown to have comparable efficiencies (15%–32%) and thrusts

^{a)}Electronic mail: asmirnov@pppl.gov

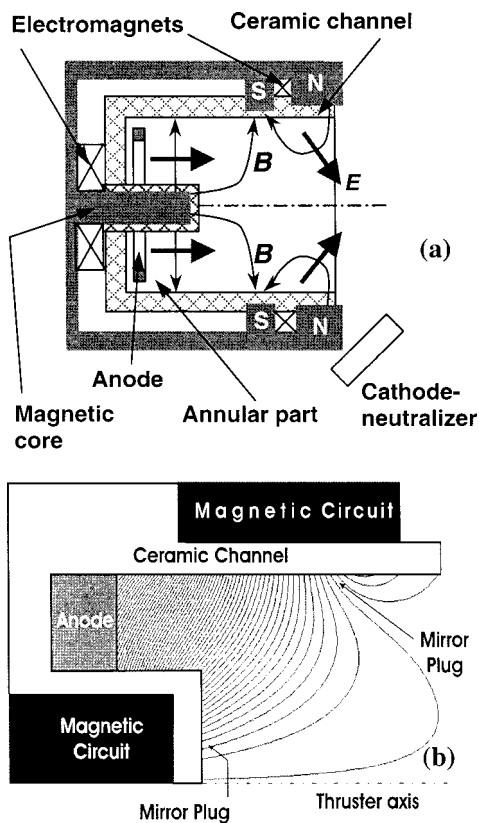


FIG. 1. (a) Schematic of a cylindrical Hall thruster. (b) Typical magnetic field distribution in a CHT.

(2.5–12 mN). It was found that both the 9 and 2.6 cm CHTs have unusually high propellant ionization efficiency, compared to conventional Hall thrusters. The ratio of the total ion current to the effective propellant mass flow current, in the case of the 2.6 cm CHT, could exceed unity, which clearly indicates the presence of multicharged Xe ions in the ion flux generated by the thruster.

The object of this article is to examine whether the effects of high propellant utilization and multicharged ion generation in the CHTs can be quantitatively explained by their lower surface-to-volume ratio, as compared with conventional geometry Hall thrusters. The article is organized as follows: In Sec. II, the main features of the 9 and 2.6 cm CHTs are presented and the experimental setup is briefly described. Section III reviews the experimental results on the propellant utilization in the CHTs. In Sec. IV, the quasi-one-dimensional (1D) Hall thruster model, developed to parametrically study the effect of wall losses reduction on a thruster operation, is described. The key results obtained in numerical simulations are presented, and their implications are discussed in Sec. V. In Sec. VI, we summarize our main conclusions.

II. EXPERIMENTAL SETUP

The 9 cm laboratory CHT is shown in Fig. 2(a). The total channel length taken from the anode to the thruster exit is 4 cm with the 1-cm-long annular part. The magnetic circuit consists of two coils connected to separate power supplies. The currents in the coils are counterdirected to produce

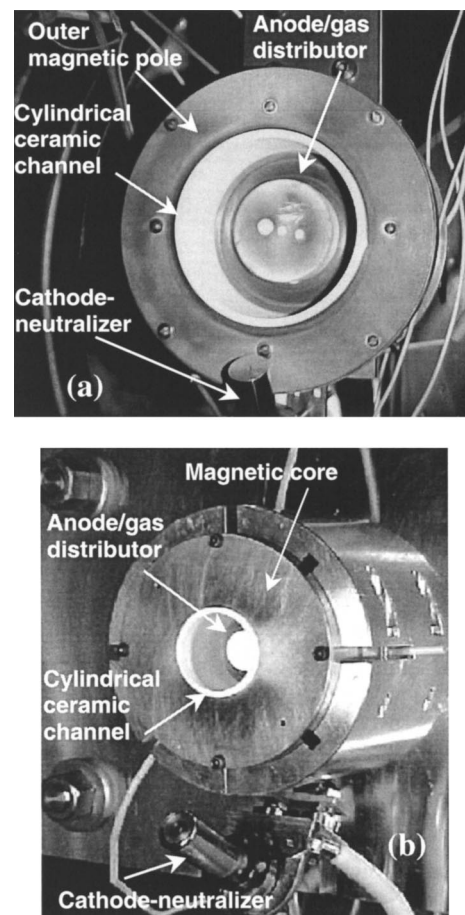


FIG. 2. (a) 9 cm and (b) 2.6 cm cylindrical Hall thrusters.

a cusp magnetic field with a strong radial component in the channel. The maximum of the radial magnetic field (about 120 G) is located near the boundary of the coaxial and cylindrical parts of the channel. In the cylindrical region, the radial magnetic field reduces towards the thruster exit. However, near the inner wall, there are two maximums of the magnetic field that are due to the opposite direction of the currents in the coils and the use of a small inner pole.

The 2.6 cm CHT, shown in Fig. 2(b), was scaled down from the 9 cm CHT to operate at about 200 W power level. The total length of the channel is 2.2 cm, the annular region is approximately 0.6 cm long. The outer and the inner diameters of the channel are 2.6 and 1.4 cm, respectively. The overall diameter and the thruster length are both 7 cm. Magnetic field profiles in the 2.6 cm CHT are similar to those in the 9 cm CHT. The radial magnetic field reaches its maximum, which is about 700 G, a few millimeters from the anode near the inner wall of the short annular part and then reduces towards the channel exit. The magnetic field was measured inside both CHTs with a miniature Hall probe with dimensions 1.5 mm×1.5 mm. The results of these measurements and simulations are in a good agreement.

The experiments were carried out in the Princeton Plasma Physics Laboratory Hall Thruster facilities: The 9 cm CHT was operated in a 28 m³ vacuum vessel, equipped with a 35 in. diffusion pump and mechanical roots pumps, and the 2.6 cm CHT was run in a 0.4 m³ vacuum chamber, equipped

with a turbomolecular pumping system. Detailed descriptions of the setups are given elsewhere.^{6,7} In the present article, we focus on the experimental setup features relevant to the propellant ionization efficiency measurements only.

The total ion flux coming from the thrusters and the plume angles were measured by movable plane electrostatic probes with guarding sleeves. The probes were made of copper–tungsten alloy for the 9 cm CHT and of graphite for the 2.6 cm CHT. Both materials have an extremely low sputtering coefficient for Xe ions with energies lower than or about 500 eV. The probes could be rotated in the vertical plane $\pm 90^\circ$ relative to the thruster exit. The probe collecting surface always pointed at the thruster center. The distance between the probe and the thruster center was 14 cm for the 2.6 cm CHT and 33 cm for the 9 cm CHT. In the experiments with the 2.6 cm CHT, yet another probe mounted on the same movable arm was used to measure the flux of backstreaming ions. The second probe was horizontally shifted about 2 cm away from the first one, and its collecting surface pointed out from the thruster. In the experiments with the 9 cm CHT, the flux of backstreaming ions was estimated from the probe currents at $\pm 90^\circ$ positions.

Flow rates of propellant, supplied to the anode and cathode, were measured by volumetrically calibrated Millipore flow controllers (0–15 and 0–10 sccm for the 2.6 cm CHT, and 0–50 and 0–10 sccm for the 9 cm CHT).

III. EXPERIMENTAL RESULTS

Results of comprehensive experimental investigations of the 9 and 2.6 cm CHTs are given in Refs. 6 and 7. Here, we discuss the thrusters propellant ionization efficiency only.

The cylindrical Hall thrusters were operated at the discharge voltage of 100–300 V and Xe mass flow rates of 1–3 mg/s (9 cm CHT) and 0.4–0.6 mg/s (2.6 cm CHT). The input power ranged from 300 to 700 W and from 50 to about 300 W for the 9 and 2.6 cm CHTs, respectively. For each CHT, it was possible to sustain the discharge under the conditions in which a discharge in a conventional annular thruster of the same size would die out due to poor propellant ionization.

The thruster ionization efficiency is characterized by a so-called propellant utilization coefficient η_I —a ratio of the total ion current I_i at the thruster exit plane to the propellant flow rate μ measured in units of electric current. Namely, $\eta_I = I_i M / e \mu$, where M is a mass of a propellant gas atom and e is the electron charge. In Fig. 3 η_I is plotted versus discharge voltage for the 9 and 2.6 cm CHTs.

The propellant utilization in the 9 cm CHT is equal to about 0.8 and varies little over the range of propellant flow rate from 1.3 to 2 mg/s. At flow rates larger than 1.7 mg/s, the propellant utilization is comparable to that in the conventional annular thruster of the same size. It did not appear possible to achieve steady-state operation of the annular thruster due to poor propellant ionization at flow rates less than 1.7 mg/s. Interestingly, the cylindrical thruster can operate stable and produce high ion flux at low propellant flow rates. Moreover, in the regimes when the current in the front thruster coil was larger than “optimal,” the propellant utili-

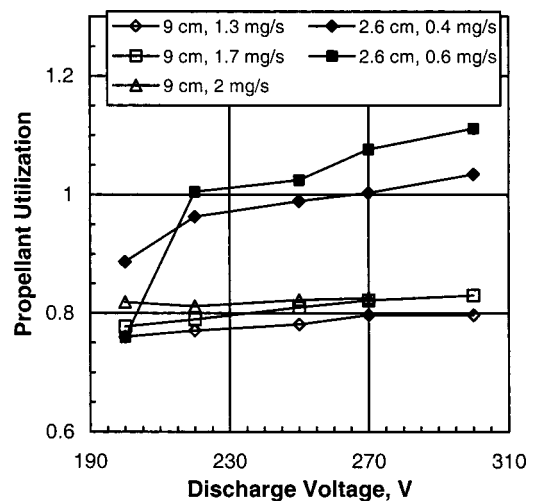


FIG. 3. Propellant utilization coefficient in the 9 and 2.6 cm cylindrical Hall thrusters at different propellant flow rates (from Refs. 6 and 7).

zation at a flow rate of 1.3 mg/s could get as high as 0.93. This indicates that propellant ionization efficiency in the cylindrical thruster at low flow rates could be higher than that in the annular thruster.

Propellant utilization for the 2.6 cm CHT can be seen to be about 20% higher than that for the 9 cm one for discharge voltages above 220 V. It increases with the discharge voltage and exceeds unity at high voltages, which implies a presence of Xe ions in charge states higher than +1 in the ion flux. As compared with the conventional annular thruster of the same size, the 2.6 cm CHT has 30%–40% higher propellant utilization coefficient at a Xe flow rate 0.4–0.6 mg/s and discharge voltages 200–300 V. It is worth mentioning also that the 2.6 CHT can be operated at a discharge voltage lower than 200 V, while for the conventional annular thruster of the same size such voltage is not sufficient to sustain the discharge at low propellant flow rates. Yet, another indication of high propellant utilization in the 2.6 cm CHT is the fact that the thrust generated in this thruster is larger than that in the 2.6 cm conventional geometry thruster.

The increase in propellant utilization in the 2.6 cm CHT might be explained by ionization enhancement due to an increase in the electron density in the discharge. The comparison between the 2.6 cm CHT and the 2.6 cm annular Hall thruster showed that the electron current to the anode in the cylindrical thruster is larger than in the annular. On the other hand, the electron anomalous mobility across the magnetic field must be lower in the cylindrical configuration, because the radial component of the magnetic field is, typically, 1.5–2 times larger than that in the annular one. Therefore, the electron density in the channel is expected to be higher in the cylindrical configuration. Simple estimates show that a 25% increase in the propellant utilization requires only about a twofold increase in the electron density. However, an increase in the radial magnetic field in a conventional annular thruster does not lead to a corresponding increase in the electron density because of the onset of strong high-frequency discharge current oscillations.⁸

The effects of high propellant utilization at low flow rates in the 9 cm CHT and enhanced ionization and multi-charged ion generation in the 2.6 cm CHT can be qualitatively explained by a lower surface-to-volume ratio of a cylindrical Hall thruster, as compared with a conventional geometry (annular) Hall thruster. Indeed, reduction of the central piece of a ceramic channel in a CHT can lead to an increase in the outgoing ion flux, because more ions can leave the channel without hitting the walls. Similarly, reduction of a wall area exposed to electrons, together with a mirror effect near the outer wall and on the axis [see Fig. 1(b)], can decrease electron energy losses on the walls and cause electron mean energy growth. Higher electron mean energy is believed to be the reason for the multicharged ion generation in the 2.6 cm CHT. The effect of a wall loss reduction on the distribution of plasma parameters in a Hall thruster is discussed in detail next.

IV. QUASI-1D THRUSTER MODEL

In order to parametrically study the effect of reduction of ion wall losses and electron energy wall losses on the distribution of plasma parameters in a Hall thruster, a quasi-1D stationary fluid model, similar to that by Ahedo *et al.*,^{9,10} was developed. The model incorporates the ion flux continuity equation with ionization and ion losses on the walls taken into account, the ion and the electron momentum equations, the Ohm's law (with a fitting parameter that accounts for Bohm diffusion), and the electron energy equation. The electron distribution function (EDF) is assumed to be Maxwellian with temperature T_e . Physical mechanisms governing the electron energy balance are Joule heating, and energy losses due to ionization and to electron escape to the walls. Heat conduction was not taken into account.

Secondary electron emission (SEE) brings about effective cooling of plasma electrons. Electron energy flux Q onto the wall can be expressed as $Q = \nu_{iw} N \epsilon_w$. Here, ν_{iw} is the plasma wall losses frequency, N is the plasma density, and ϵ_w is the energy lost per an electron-ion pair leaving the plasma. $\nu_{iw} = 2\chi V_B/h$, where χ is the density drop in the presheath, V_B is the ion Bohm velocity, and h is a channel width. ϵ_w depends on the electron temperature T_e , SEE coefficient γ , and sheath potential drop ϕ_w as $\epsilon_w = 2T_e/(1-\gamma) + |e\phi_w|$. When γ increases from 0 to 1, Q grows. However, when γ reaches some critical value $\gamma_c = 1 - \alpha(m_e/M_i)^{0.5}$ ($\gamma_c \approx 0.983$ for Xe), space charge saturation of the wall sheath occurs.¹¹ For $|\gamma|_{\text{at the wall}} > \gamma_c$, a near-wall potential well forms such that a fraction of the emitted electron flux is returned to the wall in order to maintain the effective γ in plasma equal to γ_c . Under these conditions, the potential drop between the plasma and the minimum of the potential well is about T_e/e . The potential variation near the wall that cuts off a fraction of emission current is small ($\sim 1-2$ V) and does not influence much the primary electrons energy balance. Thus, space charge saturation of the wall sheath limits the electron energy losses from plasma.

The SEE coefficient on the wall is a function of electron energy ϵ and incidence angle θ . In order to find $\gamma(T_e)$ necessary for calculations, we have to average $\gamma(\epsilon, \theta)$ over the

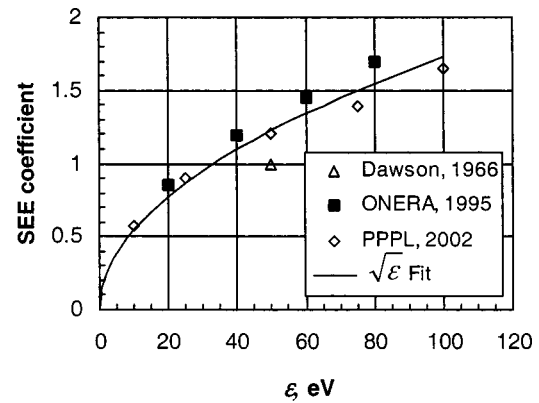


FIG. 4. Coefficient of secondary electron emission (SEE) from BN according to different sources (see Refs. 12, 13, and 14); $\sqrt{\epsilon}$ Fit—result of fitting the experimental data with function $a \times [\epsilon(\text{eV})]^{0.5}$, $a \approx 0.173$.

distribution of primary electrons on the wall. In contrast to the model described in Ref. 9, we use the data on SEE obtained in the experiment. In Fig. 4, $\gamma(\epsilon)$ from boron-nitride is plotted for all, to the best of our knowledge, reported measurements of SEE from this material.¹²⁻¹⁴

To derive a simple expression for $\gamma(T_e)$ that can be used in simulations, we fitted experimental data with function $\gamma = a \times [\epsilon(\text{eV})]^{0.5}$, and found that $a \approx 0.173$. Effective SEE yield, averaged over Maxwellian EDF, can be expressed then as

$$\gamma(T_e) = \begin{cases} \kappa \sqrt{T_e(\text{eV})}, & T_e \leq T^* \\ \gamma_c, & T_e > T^* \end{cases}$$

Here, $\kappa \approx 0.23$. $T^* \approx 18.26$ eV is a temperature at which the SEE coefficient reaches its critical value γ_c .

The channel wall acts as an extremely effective energy sink as $\gamma \rightarrow \gamma_c$. Therefore, electron energy losses on the wall are likely to limit the electron temperature in the channel at the threshold value T^* (and this, in fact, is what really happens in the numerical simulation—see Sec. V of this article). The numerical value of T^* is determined by the dependence of the SEE coefficient on the energy of primary electrons. Thus, we ascribe great importance to a thorough experimental study of secondary electron emission from Hall thruster channel materials.

V. RESULTS OF NUMERICAL SIMULATIONS AND DISCUSSION

Although we show that it is insufficient to explain the observations, one possible reason for the increase in propellant ionization efficiency and generation of multicharged ions in a CHT might be a reduction of particle and energy wall losses in the cylindrical region, as compared with an annular thruster. The magnetic field in a CHT has a two-dimensional (2D) distribution. Of course, the complex picture of physical processes that occur in the cylindrical region of a thruster cannot be quantitatively described by a quasi-1D model. However, the influence of the wall losses, considered by itself, can be modeled in a rather simple parametric way. In the numerical simulations, we focus on the case of the 2.6 cm CHT.

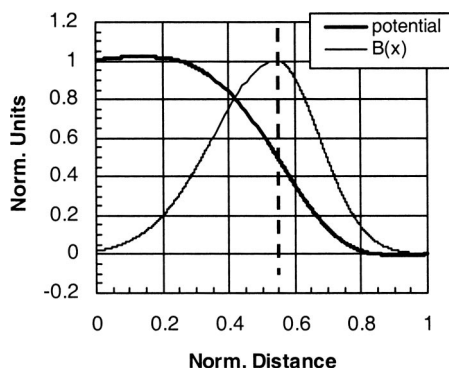


FIG. 5. Normalized magnetic field and electric potential profiles in a thruster with long walls. Normalization constants are $B_{\max}=400$ G, $\Delta\phi_{\text{tot}}=234$ V (close to the values typical for the 2.6 cm annular thruster). Normalized channel length is equal to 1. Distance is measured from the anode towards the channel exit. Wall losses are parametrically reduced to the right from the dashed lined.

We take into account two experimental facts. First, the magnetic field in the 2.6 cm CHT is concentrated in the annular part of the channel (i.e., deep inside the thruster, far from the thruster exit). Second, potential profile measurements in a 9 cm cylindrical thruster showed that most of the potential drop occurs in the cylindrical region near the edge of the annular part of the channel.⁶ Therefore, it seems relevant to study the influence of the wall losses on a model conventional geometry (annular) thruster that has: (i) the magnetic field concentrated well inside the channel and (ii) the entire potential drop located inside the channel, too (Fig. 5). We call such a model a thruster with “long” walls. For such a thruster, we can assume the cathode plane to be located at the channel exit, and avoid the problem of plume modeling. The long-wall thruster model is considered solely for the purpose of studying how the reduction of the wall losses in a conventional thruster influences its operation.

We considered a model magnetic field profile given in Fig. 5. For this model thruster, we calculated plasma parameter profiles for the discharge conditions typical of the 2.6 cm annular thruster.⁷ Boundary conditions used for numerical simulations are the following. Ion velocity at the anode is equal to $-V_B$. The regime with no anode sheath, which can be realized at high discharge voltages,¹⁵ was not considered. The plasma density at the anode is selected so that to give a solution with a smooth transition of ion fluid velocity through a sonic point. Electron temperature at the cathode plane (channel exit) is taken to be equal to 4–5 eV, which is an experimentally observed value.¹⁶ As an example of a calculation, the thick line in Fig. 5 shows the electric potential distribution. The discharge conditions are: Maximum radial magnetic field $B_{\max}=400$ G, total potential drop in the channel $\Delta\phi_{\text{tot}}=234$ V, propellant flow $\mu=0.6$ mg/s, and discharge current $I_d=0.605$ A.

In order to see what happens to the propellant utilization if the plasma wall losses are reduced in the region with strong electric field, we parametrically decreased the plasma wall losses in the region from the magnetic field maximum up to the channel exit (to the right from the dashed line in Fig. 5). Note that the total electric potential drop in this

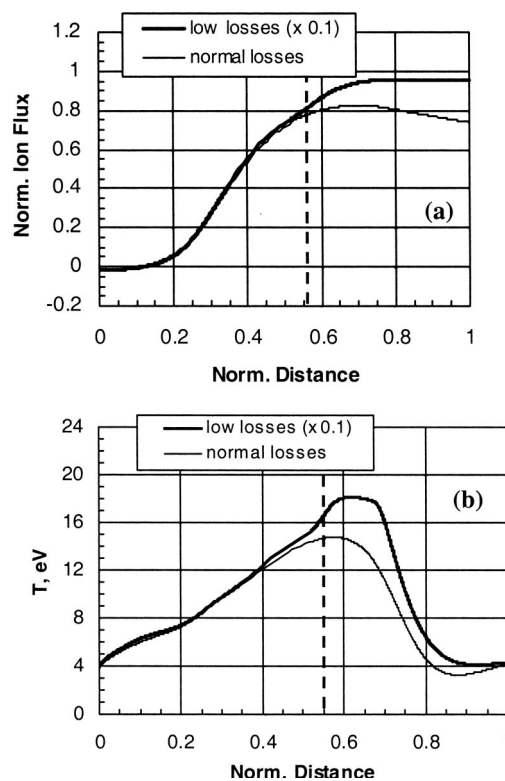


FIG. 6. (a) Ion current normalized by the propellant flow rate and (b) temperature profiles for the thrusters with normal and decreased wall losses. Losses are reduced by an order of magnitude to the right from the dashed line. Space-charge saturation of the wall sheaths occurs in the interval of normalized distance from ~ 0.58 to ~ 0.67 . $B_{\max}=400$ G, $\Delta\phi_{\text{tot}}=234$ V, and $\mu=0.6$ mg/s. Discharge current is equal to 0.605 A for normal losses and 0.63 A for low losses. Distance is measured from the anode towards the channel exit.

region is significant, and equals to about a half of the applied discharge voltage. We modeled the reduction of both ion wall losses and electron energy wall losses by multiplying the frequency of plasma escape to the wall ν_{iw} by a coefficient less than unity.

Elimination of the inner wall in the 2.6 cm CHT decreases the area exposed to the plasma by a factor of approximately 2. In addition, there may be some reduction in the rate of electron escape to the outer wall due to the mirror effect [see Fig. 1(b)]. However, it does not seem feasible to estimate accurately what the actual overall decrease of the losses in the cylindrical thruster is. Therefore, to see what the ultimate effect of the wall losses reduction is, we consider a model situation with the wall losses reduced by an order of magnitude. In Fig. 6, the results of the corresponding calculations are shown. We compare two cases: (i) “normal” wall losses, i.e., real wall losses in the long-wall thruster; discharge conditions are the same as in Fig. 5, and (ii) “low” losses, i.e., losses reduced by a factor of 10; B_{\max} , $\Delta\phi_{\text{tot}}$, and μ are kept the same as in the low loss case.

As follows from Fig. 6(a), an order of magnitude reduction of wall losses leads to approximately 20% increase in the propellant utilization. This is only about a half of the experimentally observed increase in the propellant utilization in the 2.6 cm CHT, as compared with the 2.6 cm annular thruster. Calculations with the wall losses reduced by a factor

of 2 (as if the reduction was due only to the elimination of the inner wall) give the propellant utilization increase of only a few percent. Thus, the experimentally observed increase in the propellant utilization does not appear to be explained in a quasi-1D model by a reduction of wall losses only. The reason for this seems to be the electron temperature limitation imposed by a space-charge saturation of the wall sheaths.

As can be seen in Fig. 6(b), in the region where the wall losses are reduced, the electron temperature gets limited at the value close to $T^* \approx 18.26$ eV. As discussed herein, it is the electron energy losses on the wall that become very strong when $\gamma \rightarrow \gamma_c$, and limit the electron temperature. The effect of the electron temperature limitation due to space-charge saturation of the wall sheaths was also observed by other authors.⁹ However, due to the realistic SEE data that we used, the temperature limitation occurred at a much lower level, as compared with the result obtained in Ref. 9. Note that $T_e \sim 18$ eV is apparently insufficient for generation of multicharged Xe ions.

The effect of the electron temperature saturation at the relatively low value of about 18 eV is a consequence of the assumption that the EDF is Maxwellian. In fact, wall collisions depopulate the tail of the EDF,¹⁷ thus strongly reducing the effective SEE coefficient and energy losses on the wall. Critical value γ_c of SEE coefficient might be achieved at a higher mean energy of the EDF bulk, than predicted by simple averaging of $\gamma(\epsilon)$ over the Maxwellian. Accurate description of experimentally observed effects requires, therefore, kinetic analysis of EDF formation and self-consistent treatment of electron heating, scattering, and wall losses. This complex problem is a subject of ongoing theoretical research.

VI. CONCLUSIONS

Annular conventional Hall thrusters become inefficient when scaled to small sizes because of the large surface-to-volume ratio and the difficulty in miniaturizing the magnetic circuit. An alternative approach, which may be more suitable for scaling to low power, is a cylindrical Hall thruster. Both the 9 cm CHT, operated in subkilowatt power range, and the miniature 2.6 cm CHT, operated in the power range 50–300 W, exhibit performances comparable with conventional annular Hall thrusters of the similar sizes. The cylindrical thrusters, however, have unusually high propellant ionization efficiency, compared to conventional Hall thrusters. Significantly, a large fraction of multicharged xenon ions might be present in the outgoing ion flux generated by the 2.6 cm CHT. The 9 cm CHT can operate stable and produce high ion flux at propellant flow rates below 1.7 mg/s, while a discharge in a 9 cm conventional thruster at such low flow rates dies out due to poor propellant ionization. The 2.6 cm CHT can be operated at the discharge voltage lower than 200 V, while for the conventional annular thruster of the same size such voltage is not sufficient to sustain the discharge at low propellant flow rates.

A possible reason for the increase in propellant utilization and generation of multicharged ions in the cylindrical thrusters is a reduction of particle and energy wall losses in the cylindrical region, as compared with the conventional annular thrusters. However, this reason is not supported by a simple quasi-1D stationary thruster model. Our numerical simulation showed that the space-charge saturation of a wall sheath limits the temperature of Maxwellian electrons at the value insufficient for strong ionization and multicharged ions generation. Therefore, the increase in the propellant utilization does not appear to be quantitatively explained by a reduction of plasma wall losses. To explain the experimentally observed effect might, in fact, require a kinetic treatment of electrons.

ACKNOWLEDGMENTS

The authors would like to thank Dr. I. Kaganovich, L. Dorf, and D. Staack for very helpful discussions and comments on this article. This work was supported by grants from AFOSR, DARPA, and U.S. DOE Contract No. AC02-76CH0-3073.

- ¹J. Ashkenazy, Y. Raitses, and G. Appelbaum, in *Proceedings of the 2nd International Spacecraft Propulsion Conference, Noordwijk, The Netherlands* (European Space Agency, Noordwijk, the Netherlands, 1997), p. 46.
- ²V. Hruba, J. Monheiser, B. Pote, C. Freeman, and W. Connolly, in *Proceedings of the 26th International Electric Propulsion Conference, Kitakyushu, Japan* (Electric Rocket Propulsion Society, Cleveland, OH, 1999), IEPC 99-092.
- ³D. Jacobson and R. Jankovsky, in *Proceedings of the 34th Joint Propulsion Conference, Cleveland, Ohio* (American Institute of Aeronautics and Astronautics, Reston, VA, 1998), AIAA 98-3792.
- ⁴O. Gorshkov, in *Proceedings of the 34th Joint Propulsion Conference, Cleveland, Ohio* (American Institute of Aeronautics and Astronautics, Reston, VA, 1998), AIAA Paper No. 98-3929.
- ⁵V. Khayms and M. Martinez-Sanches, in *Micropropulsion for Small Spacecraft, Progress in Astronautics and Aeronautics*, edited by M. M. Micci and A. D. Ketsdever (American Institute of Aeronautics and Astronautics, Reston, VA, 2000), Vol. 187, p. 45.
- ⁶Y. Raitses and N. J. Fisch, *Phys. Plasmas* **8**, 2579 (2001).
- ⁷A. Smirnov, Y. Raitses, and N. J. Fisch, *J. Appl. Phys.* **92**, 5673 (2002).
- ⁸J. P. Boeuf and L. Garrigues, *J. Appl. Phys.* **84**, 3541 (1998).
- ⁹E. Ahedo, J. M. Gallardo, and M. Martinez-Sanchez, in *Proceedings of the 38th Joint Propulsion Conference, Indianapolis, Indiana* (American Institute of Aeronautics and Astronautics, Reston, VA, 2002), AIAA 2002-4244.
- ¹⁰E. Ahedo, J. M. Gallardo, and M. Martinez-Sanchez, *Phys. Plasmas* **9**, 4061 (2002).
- ¹¹G. D. Hobbs and J. A. Wesson, *Plasma Phys.* **9**, 85 (1967).
- ¹²P. H. Dawson, *J. Appl. Phys.* **37**, 3644 (1966).
- ¹³J. P. Bugeat and C. Koppel, in *Proceedings of the 24th International Electric Propulsion Conference, Moscow, Russia* (Electric Rocket Propulsion Society, Cleveland, OH, 1995), IEPC 95-35.
- ¹⁴A. Dunaevsky, Y. Raitses, and N. J. Fisch, *Phys. Plasmas* **10**, 2574 (2003).
- ¹⁵L. Dorf, V. Semenov, Y. Raitses, and N. J. Fisch, in *Proceedings of the 38th Joint Propulsion Conference, Indianapolis, Indiana* (American Institute of Aeronautics and Astronautics, Reston, VA, 2002), AIAA 2002-4246.
- ¹⁶A. M. Bishaev and V. Kim, *Sov. Phys. Tech. Phys.* **23**, 1055 (1978).
- ¹⁷I. Kaganovich, M. Misina, S. V. Berezhnoi, and R. Gijbels, *Phys. Rev. E* **61**, 1875 (2000).